# REFERENCES


Acros Organics BVBA Inc. "Material Safety Data Sheet, trans-Cinnamic acid, 98+%" 26 Jan. 2012. <https://ecat.fishersci.ca/%28S%28tutgcn45x1ejhlqh1lz4grz4%29%29/ViewMSDS.aspx?cat=AC158575000>.

Allen, J.R.L. (1971). Bed forms due to mass transfer in turbulent flows: a kaleidoscope of phenomena. Journal of Fluid Mechanics, 49(1), 49-63.

Allen, J.R.L. (1971). Transverse erosional marks of mud and rock: their physical basis and geological significance. Sedimentary Geology, 5, 167-385.

Arzutuğ, M. E., Yapici, S. and M. Kocakerim, M. M. (2005). A comparison of mass transfer between a plate and submerged conventional and multichannel impinging jets. International Communications in Heat and Mass Transfer, 32, 852-854.

"Aspartic acid", New World Encyclopedia 4 Apr. 2012. <http://www.newworldencyclopedia.org/entry/Aspartic_acid>

Azimi, A., Papangelakis, V.G. and Dutrizac, J.E. (2007). Modelling of calcium sulphate solubility in concentrated multi-component sulphate solutions. Fluid Phase Equilibria, 260, 300-315.

B. Stellwag (1998). The mechanism of oxide film formation on austenitic stainless steels in high temperature water. Power Plant Chemistry and Decontamination, Siemens AC Power Generation (KWU), Erlangen, Federal Republic of Germany, 337-370.

Blumberg, P.N. and Curl R.L. (1974). Experimental and theoretical studies of dissolution roughness. Journal of Fluid mechanics, 65(4), 735-751.

Budavari, Susan, ed. (1996). The Merck Index: An Encyclopedia of Chemicals, Drugs, and Biologicals (12th ed.), Merck, ISBN 0911910123.

Colombani J. and Bert J. (2007). Holographic interferometry study of the dissolution and diffusion of gypsum in water. Geochimica et Cosmochimica Acta, 71, 1913–1920.

Cheng, Y.F. and Steward, F.R. (2004). Corrosion of carbon steels in high-temperature water studied by electrochemical techniques. Corrosion Science, 46 2405–2420.

Chin, D. and Hsueh, K. (1986). An analysis using the Chilton-Colburn analogy for mass transfer to flat surface from an unsubmerged impinging jet. Electrochemica Acta, 31(5), 561.

Chin, D. T. and Tsang, C.H. (1978). Mass transfer to an impinging jet electrode, Journal of the Electrochemical Society, 125(9), 1470.

"Corrosion Control in Engineering Design". 23 May. 2011. <http://www.npl.co.uk/upload/pdf/corrosion_control_in_engineering_design.pdf>.

"Corrosion Rate Conversion Factors". Processassociates.com. 23 May. 2011. <http://www.processassociates.com/process/convert/cf_cor.htm>.

"Corrosion Rate Conversion". 23 May. 2011. <http://www.corrosionist.com/corrosion_rate_conversion.htm>.

"Corrosion Theory". NACE Resource Center. 23 May. 2011. <http://events.nace.org/Library/corrosion/Principles/Theory.asp>.

Curl, R.L. (1974). Deducing flow velocity in cave conduits from scallops. The NSS Bulletin, 36(2), 1-5.

"Definition of Corrosion". NASA – Corrosion control and treatment manual - TM-584C revision C. 23 May. 2011. <http://www.corrosionist.com/definition_of_corrosion.htm>.

Delgado J. M. P. Q. (2007), Molecular Diffusion Coefficients of Organic Compound in Water at Different Temperatures. Journal of Phase Equilibria and Diffusion, Vol. 28 No. 5.

Edward J. Bennett Company. (2005), "Dial Indicator Primer" 2 Dec. 2011. <http://www.ts-aligner.com/dialindicator.htm >re

"EDX - Energy Dispersive X-ray Analysis" GlobalSino.17Apr. 2011. 23 May. 2011. <http://www.globalsino.com/micro/1/micro9999.html>

Efird, K.D., Wright E.J., Boros, J.A. and Hailey, T.G. (1993). Correlation of Steel Corrosion in Pipe Flow with Jet Impingement and Rotating Cylinder Tests. Corrosion Engineering, 49(12), 992-1002.

Fisher Scientific Company"Material Safety Data Sheet, L-Aspartic Acid" 4 Apr. 2012. <https://www.fishersci.ca/ViewMSDS.aspx?cat=BP374100&lang=EN>

Fisher Scientific Company"Material Safety Data Sheet, L(+)-Potassium hydrogen tartrate, 99%" 4 Apr. 2012. <https://ecat.fishersci.ca/%28S%28fbxst555zea1ir55bbmjxobb%29%29/ViewMSDS.aspx?cat=AC222670010>

"Flow Accelerated Corrosion Simulator/Monitor" Jonas, Inc. 2009. 23 May. 2011. <http://www.steamcycle.com/facmonitor.htm>

Gardiner, D.J. (1989). Practical Raman spectroscopy. Springer-Verlag, ISBN 978-0387502540.

Grundke, G. (1976). Grundriß der allgemeinen Warenkunde. Bd. III, VEB Fachbuchverlag, Leipzig, 4. Aufl.

Hauffe, K. (1966) Reaktionen in und anfestenStoffen, 2nd edn. Springer-Verlag, Berlin.

Henderson, E.P. and Perry, S.H. (1958). Studies on siderites. Proc.U.S. Natl. Museum, 107, 339-403.

James, A.N. and Lupton, A.R.R. (1978). Gypsum and anhydrite in foundations of hydraulic structures. Geotechique, 28(3), 249-272.

Jeschke, A.A., Vosbeck, K. and Dreybrodt, W. (2001). Surface controlled dissolution rates of gypsum in aqueous solutions exhibit nonlinear dissolution kinetics. Geochimica et Cosmochimica Acta, 65(1), 27-34.

Jung, S. K. and Pierrefeu D. L. (2010). Electrochemical characterization of sintered magnetite electrode in LiOH solution. Corrosion Science, 52, 817–825.

Kain, V., Roychowdhurya, S., Mathew, T. and Bhandakkar, A. (2008). Flow accelerated corrosion and its control measures for the secondary circuit pipelines in Indian nuclear power plants. Journal of Nuclear Materials, 383, 86–91.

Konstantin, L. "Bragg's Law and Diffraction: How waves reveal the atomic structure of crystals" 2010. 30 Jun. 2011. <http://www.eserc.stonybrook.edu/ProjectJava/Bragg/>.

Koshizuka, S., Naitoh, M., Uchida,S. and Okada, H. (2010). Evaluation Procedures for Wall Thinning due to Flow Accelerated Corrosion and Liquid Droplet Impingement. International Symposium on the Ageing Management & Maintenance of Nuclear Power Plants, 18-28.

Lebedev, A.L. and Lekhov, A.V. (1989). Dissolution kinetics of natural-gypsum in water at 5-25°C. Moscow University. 6: 865-874.

Leighly, J. (1948). Cuspate surfaces of melting ice and firn. Geograph. Rev., 38:300-306.

Lertsurasakda, C. (2007). The effect of surface scalloping on flow hydrodynamics and pressure drop. M.S. Thesis, The Petroleum and Petrochemical Collage, Chulalongkorn University.

Lister, D.H., Davidson, R.D. and McAlpine E. (1987). Corros.Sci., 27, 113-140.

Lister, D.H., Liu, L., Feicht, A., Khatibi, M., Cook, W., Fujiwara, K., Kadoi, E., Ohira, T., Takiguchi, H. and Uchida, S. (2008). Flow-Accelerated Corrosion in Feedwater Systems. 15th International Conference on the Properties of Water and Steam (15th ICPWS), Berlin, Germany, 1-9.

Lui, S. and Nancollas, G.H. (1971). The kinetics of dissolution of calcium sulfate dehydrate. Journal of Inorganic Nuclear Chemistry, 33, 2311-2316.

Luttikul A. (2010). Oxide film characteristics under PWR primary coolant . M.S. Thesis, The Petroleum and Petrochemical Collage, Chulalongkorn University.

McBee, C.L. and Kruger (1972). J. Electrochim. Acta, 17, 1337-1341.

Mineral Data Publishing, (2005). Gypsum, 1, 1.

Naitoh, M., Uchida, S., Koshizuka, S., Ninokata, H., Hiranuma, N., Dosaki, K.,Nishida, K., AkiyamaM. and H. Saitoh (2008). Evaluation Methods for Corrosion Damage of Components in Cooling Systems of Nuclear Power Plants by Coupling Analysis of Corrosion and Flow Dynamics is (I), Major targets and development strategies of the evaluation methods. Journal Nuclear Science Technology, 45, 1116.

Nasrazadani, S., Nakka, R.K., Hopkins, D. and Stevens, J. (2009). Characterization of oxides on FAC susceptible small-bore carbon steel piping of a power plant. International Journal of Pressure Vessels and Piping, 86, 845–852.

Opdyke, N.B., Gust, G. and Ledwell, R.J. (1987) Mass transfer from smooth alabaster surfaces in turbulent flows. Geophysical research letters, 14(11), 1131-1134.

Pattanaparadee, T. (2007). Characterization of oxide flim on CANDU Reactor feeder pipe steel in high temperature water. M.S. Thesis, The Petroleum and Petrochemical Collage, Chulalongkorn University.

PerkinElmer, Inc. (2007). Introduction to Raman Spectroscopy, 1-7.

Pierrefeu, D. L. (2009) The dissolution behavior of magnetite electrodes in high-temperature water. Master of Science in Engineering thesis, University of New Brunswick.

"Potassium Bitartrate", BookRags, Inc. 4 Apr. 2012. <http://www.bookrags.com/research/potassium-bitartrate-chmc>

Princeton instrument, (2011). Raman Spectroscopy Basics., 1-5.

Raines, M. and Dewer, T. (1997). Mixed kinetics control of fluid-rock interaction in reservoir production senarios. Journal of Petroleum Science and Engineering, 17, 139-155.

Rao, V. V. and Trass, O. (1964) Mass transfer from a flat surface to an impinging turbulent jet. The Canadian Journal of Chemical Engineering, 95-99.

Rechenberg, W. and Sprung, S. (1983) Composition of the solution in the hydration of cement. Cement and Concrete Research, 13, 119-126.

Scintag Inc., (1999). Basics of X-ray Diffraction., 1-25.

Shao, Y. (2006) The scalloping phenomenon and the influence of oxygen on flow accerated corrosion in feed water systems. Master of Science in Engineering thesis, University of New Brunswick.

Sharp, J.P. (1974) The wolf-creek glaciers, St Elias Range, Yukorn Territory. Geograph. Rev., 37, 26-52.

Sinthuphan, S. (2008). Effect of dissolution rate and flow characteristics on scalloping of pipe surfaces. M.S. Thesis, The Petroleum and Petrochemical Collage, Chulalongkorn University.

Song, R.H., Pyun, S.I. and Oriani R.A. (1990) Journal of Electrochemical Society, 137, 1703.

Swapp, S. “Scanning Electron Microscopy (SEM)” University of Wyoming. 23 May. 2011.<http://serc.carleton.edu/research_education/geochemsheets/techniques/SEM.html>.

Taylor and Francis Group, LLC (2011), CRC Handbook of Chemistry and Physics 91 st Edition.

“The mineral gypsum”. Amethyst Galleries Inc. 30 Jun. 2011. <http://www.galleries.com/minerals/sulfates/gypsum/gypsum.htm>.

“Types of Corrosion”. 23 May. 2011. <http://www.counteractrust.com/types%20of%20corrosion.htm>.

Villien, B., Zeng Y. and Lister, D. H. (2001). The Scalloping Phenomenon and its Significance in Flow Assisted-Corrosion. Twenty Sixth Annual CNS-CAN Student Conference, Toronto, Canada.

Villien, B., Zheng, Y. and Lister D.H. (2005). Surface dissolution and the development of scallops. Chem. Eng. Comm., 192, 125-136.

Villien, B. (2001) The scalloping phenomenon and its significance in flow-assisted corrosion. Master of Science in Engineering thesis, University of New Brunswick.

Wallace, A. G., “Solubility of Cal-CM Plus™ (Concentrated Minerals)” 2003. 30 Jun. 2011. <http://www.awgypsum.com/solubility.htm>.

Warunphaisal, P. (2009). Surface dissolution and formation of Scallops. M.S. Thesis, The Petroleum and Petrochemical Collage, Chulalongkorn University.

Welty, J. R., Wicks, C. E., Wilson, R. E., and Rorrer, G. L (2007). Fundamentals of Momentum, Heat, and Mass Transfer 5th Edition, Department of Mechanical Engineering, Oregon State University.

“X-ray diffraction (XRD) PHILIPS X'Pert instrument and software package”, Materials and Engineering Research Institute, Sheffield Hallam University, UK 2010. 30 Jun. 2011. <http://www.shu.ac.uk/research/meri/equipment/xrd.html>.

“X-ray Diffraction” PANalytical, B.V. 30 Jun. 2011. <http://www.panalytical.com/index.cfm?pid=135>.

Zhu. H., Yang D. and Zhu L. (2006). Hydrothermal growth and characterization of magnetite (Fe3O4) thin films. Surface & Coatings Technology, 201, 5870–5874.

Zinemanas, D. and Herszage, A. (2008). Flow Accelerated Corrosion: Flow field and mass transport in bifurcations and nozzles. Chief Chemist Department, Department of Energy Technologies Development, The Israel Electric Corporation Ltd.

# APPENDICES

## Appendix A Pellet Profiles

Surface profilometry (Surtronic 25 and dial indicator) was used to determine the roughness of pellet surfaces and to measure the extent of dissolution; in order to calculate the volume loss. The commercial plaster pellets were assumed as a paraboloid form while other materials were used the actual profile to calculate.

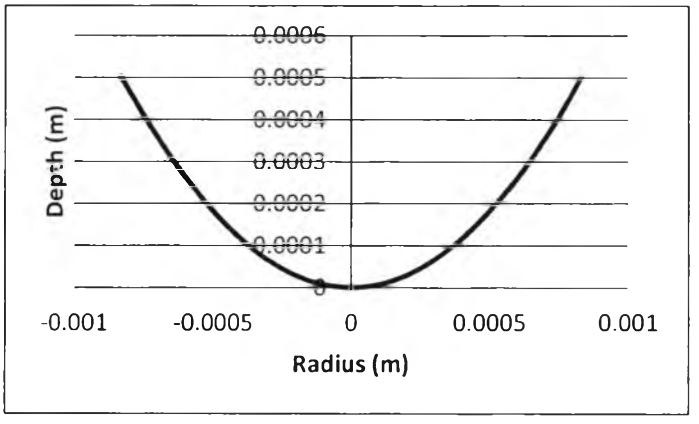


**Figure A.1** Commercial plaster profile at 40 ml/min and 25°C.

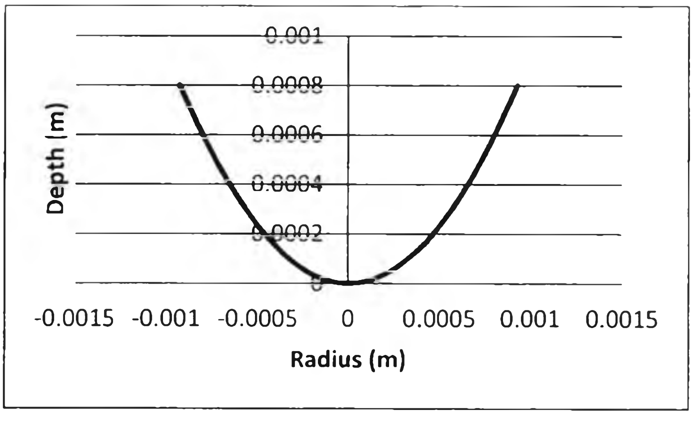


**Figure A.2** Commercial plaster profile at 60 ml/min and 25°C.

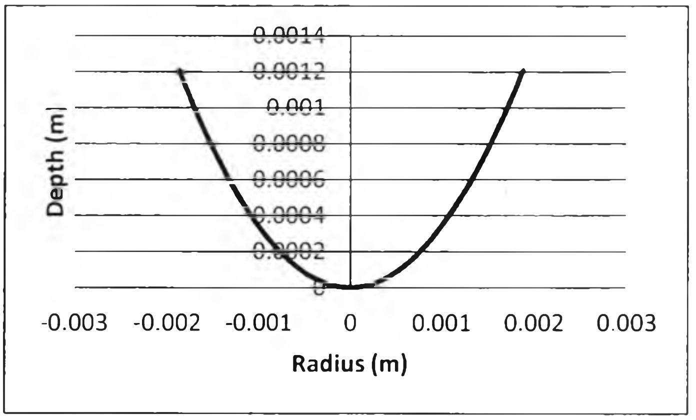


**Figure A.3** Commercial plaster profile at 80 ml/min and 25°C.

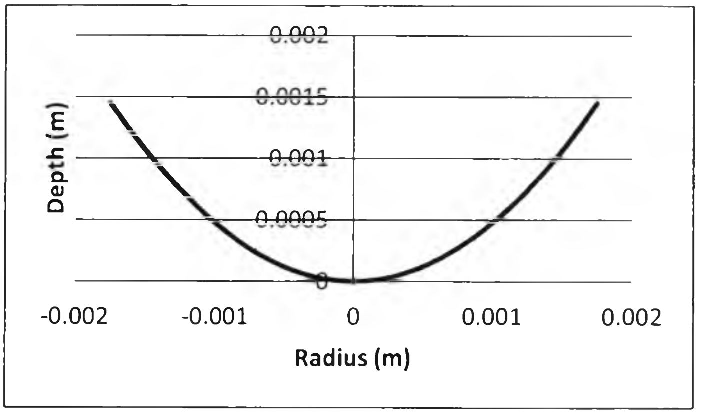


**Figure A.4** Commercial plaster profile at 100 ml/min and 25°C.

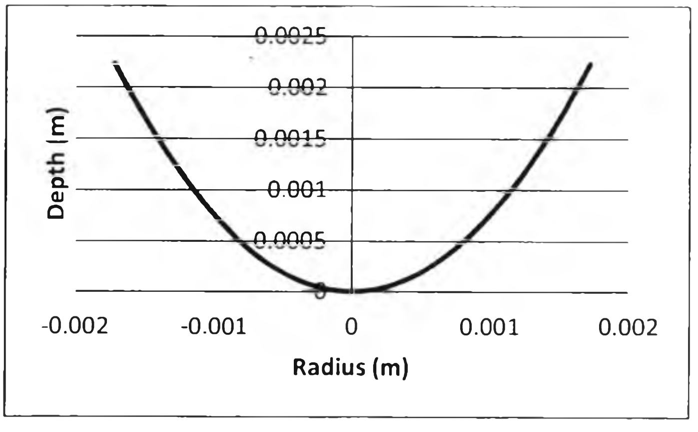


**Figure A.5** Commercial plaster profile at 120 ml/min and 25°C.

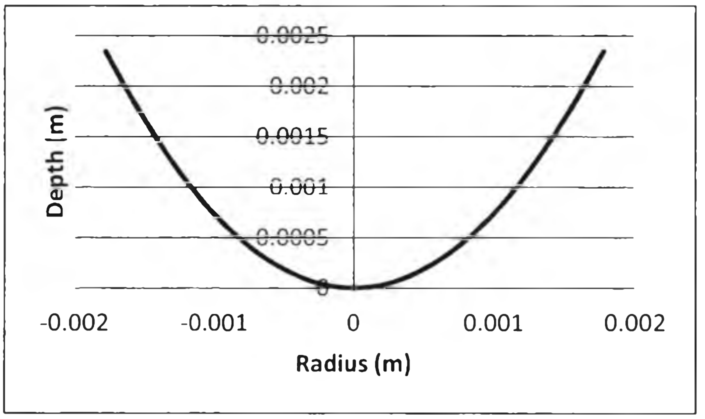


**Figure A.6** Commercial plaster profile at 140 ml/min and 25°C.

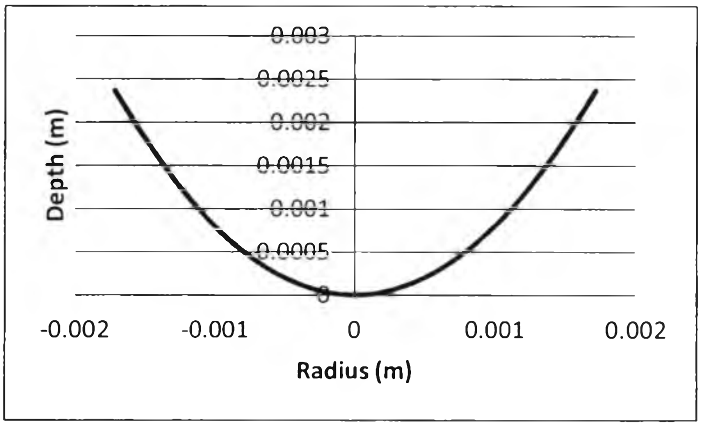


**Figure A.7** Commercial plaster profile at 160 ml/min and 25°C.

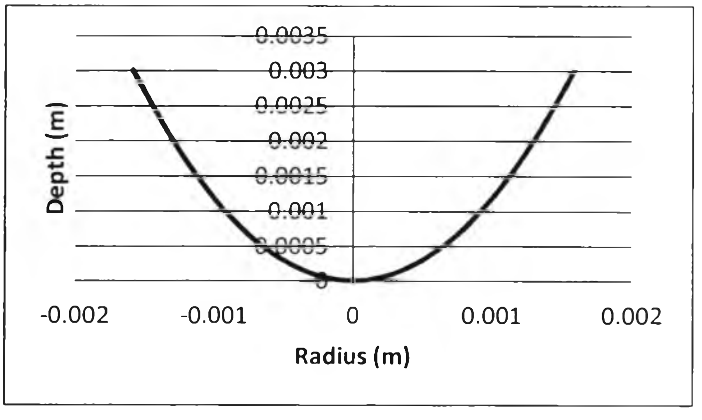


**Figure A.8** Commercial plaster profile at 180 ml/min and 25°C.

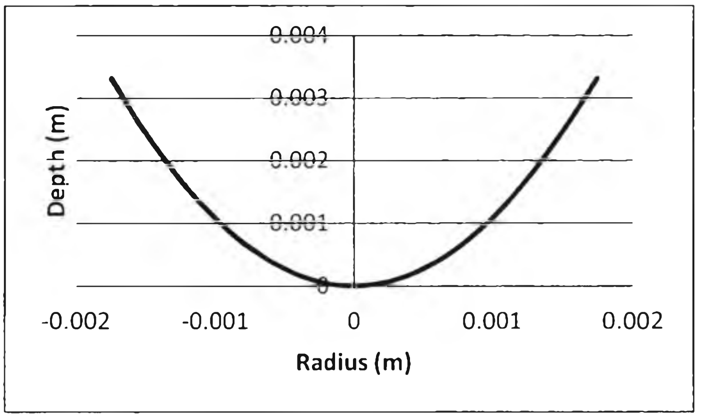


**Figure A.9** Commercial plaster profile at 199 ml/min and 25°C.

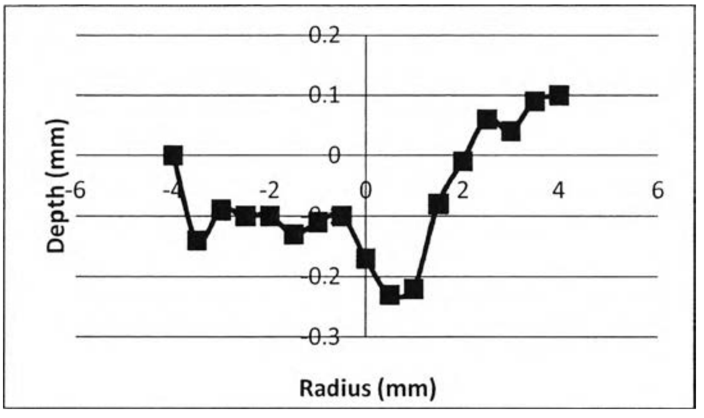


**Figure A.10** Pure plaster profile at 40 ml/min and 35°C.

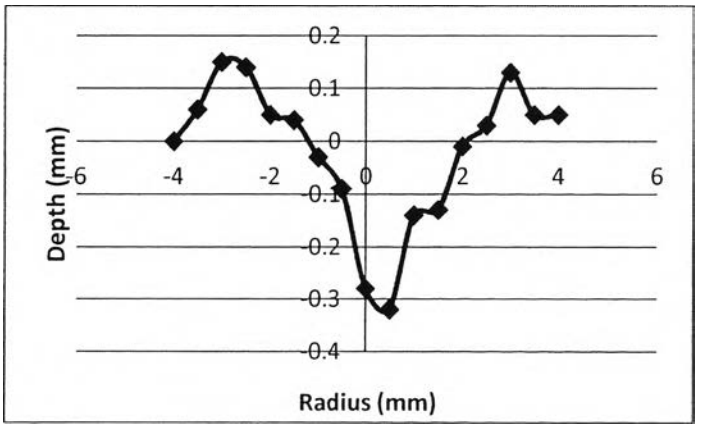


**Figure A.11** Pure plaster profile at 60 ml/min and 35°C.

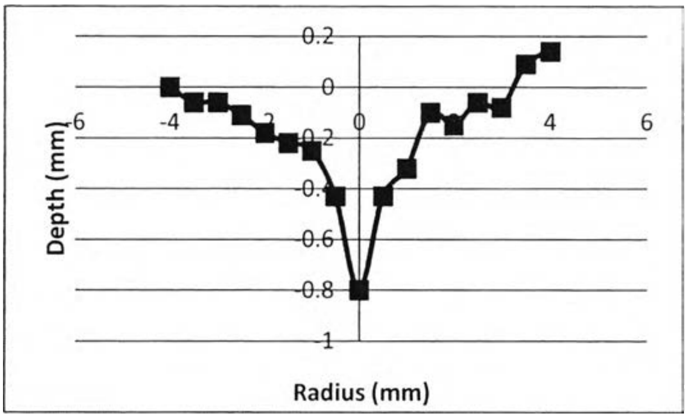


**Figure A.12** Pure plaster profile at 80 ml/min and 35°C.

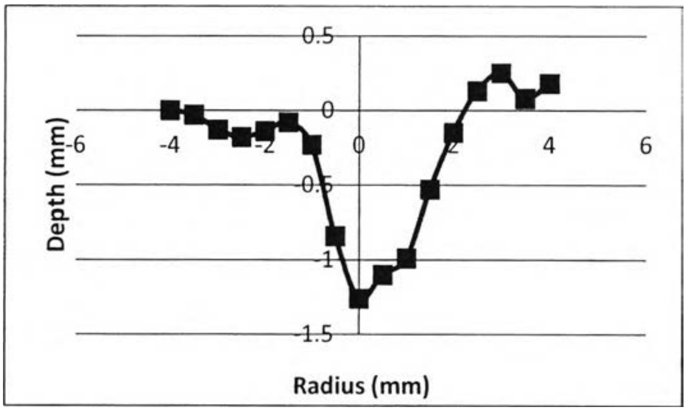


**Figure A.13** Pure plaster profile at 100 ml/min and 35°C.

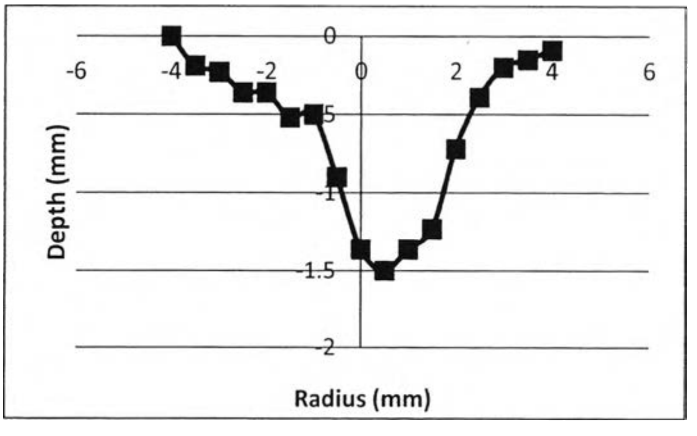


**Figure A.14** Pure plaster profile at 120 ml/min and 35°C.

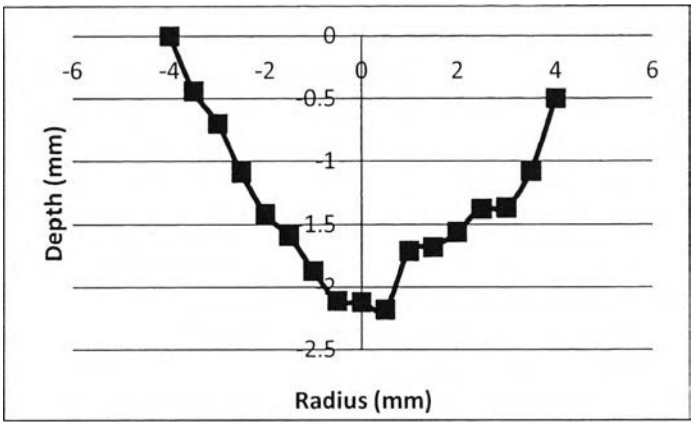


**Figure A.15** Pure plaster profile at 140 ml/min and 35°C.

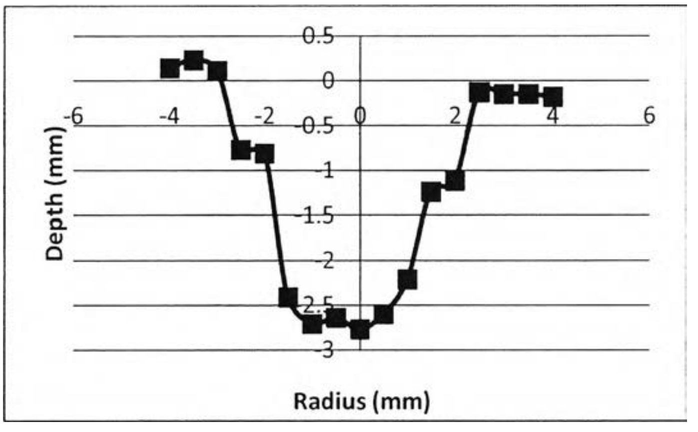


**Figure A.16** Pure plaster profile at 160 ml/min and 35°C.

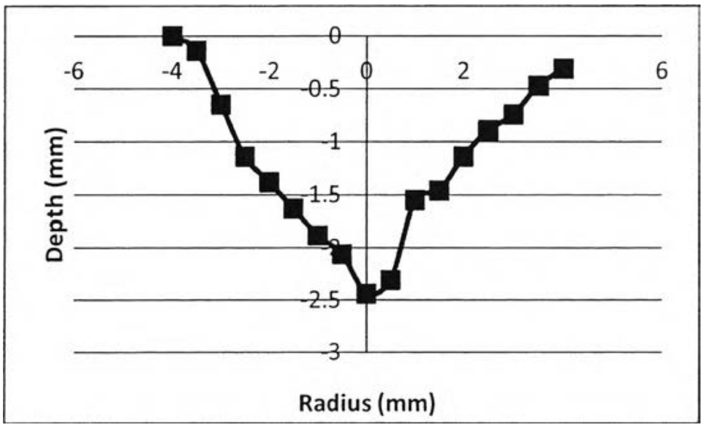


**Figure A.17** Pure plaster profile at 180 ml/min and 35°C.

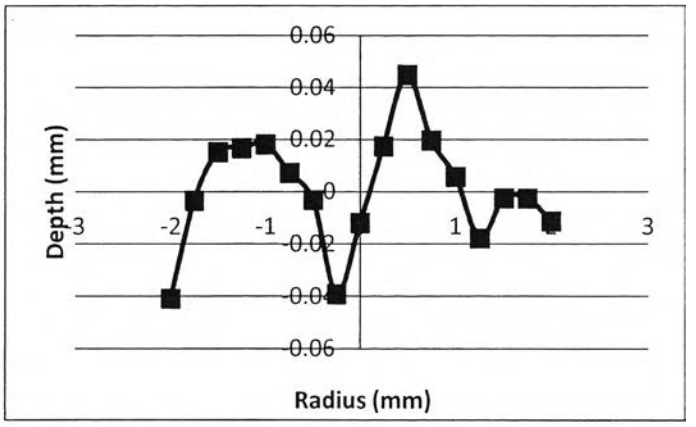


**Figure A.18** Small single crystal profile at 120 ml/min and 20°C.

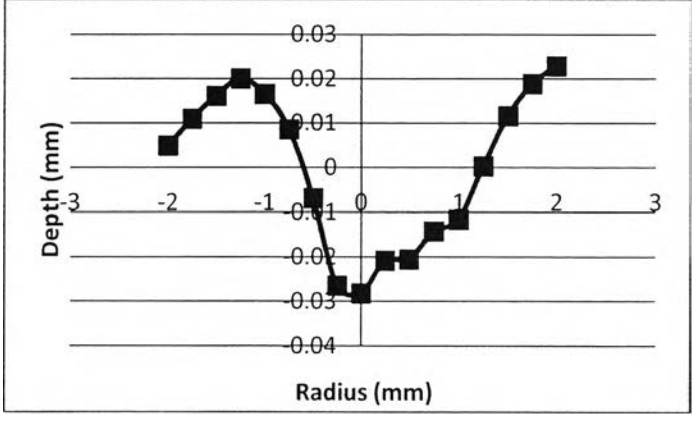


**Figure A.19** Big single crystal profile at 120 ml/min and 20°C.

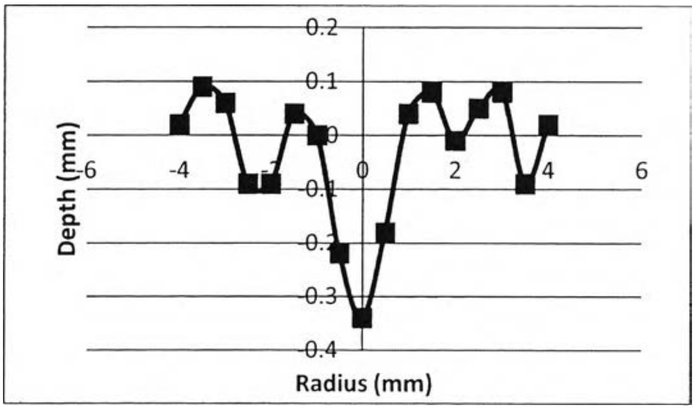


**Figure A.20** Potassium bitatrate profile at 40 ml/min and 20°C.

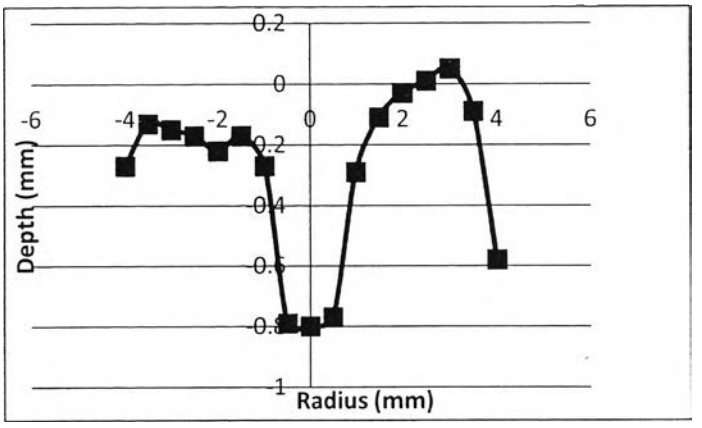


**Figure A.21** Potassium bitatrate profile at 60 ml/min and 20°C.

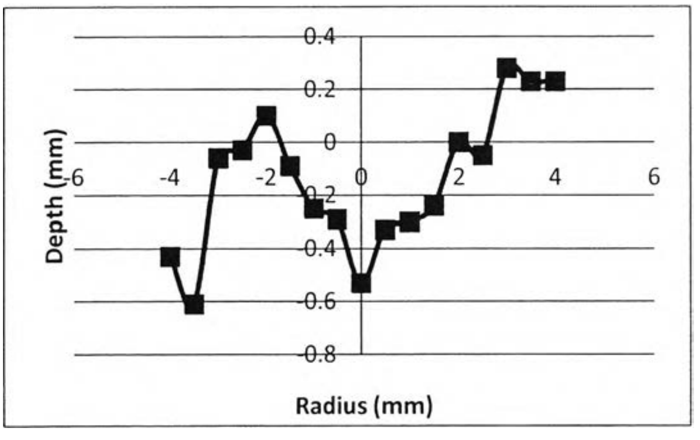


**Figure A.22** Potassium bitatrate profile at 80 ml/min and 20°C.

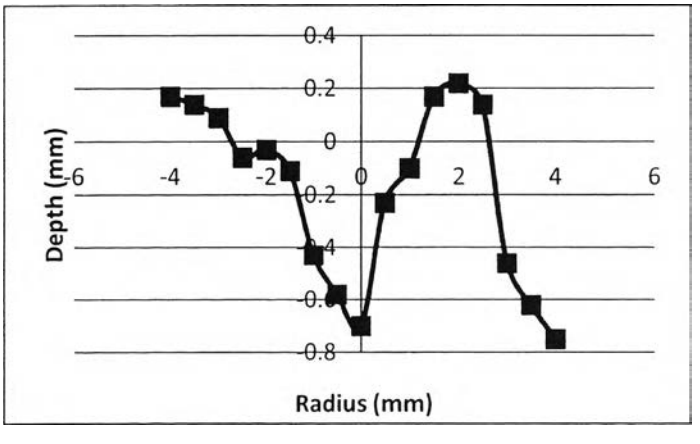


**Figure A.23** Potassium bitatrate profile at 100 ml/min and 20°C.

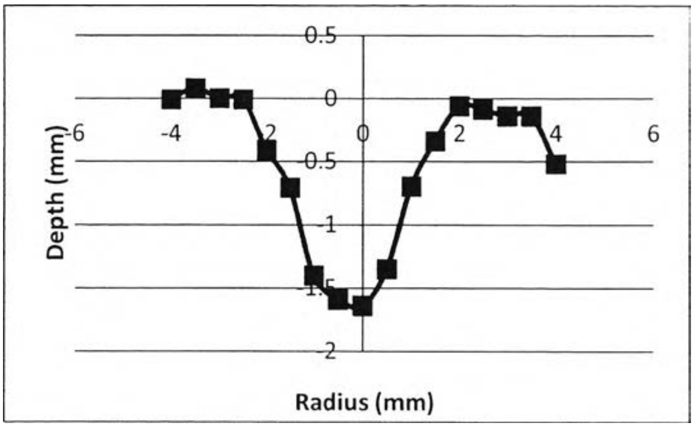


**Figure A.24** Potassium bitatrate profile at 120 ml/min and 20°C.

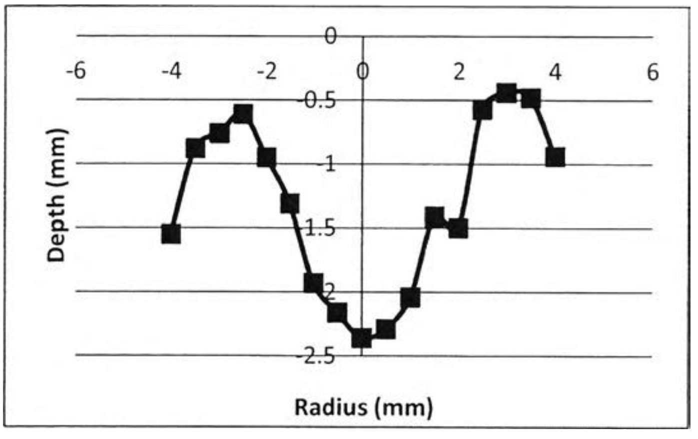


**Figure A.25** Potassium bitatrate profile at 140 ml/min and 20°C.

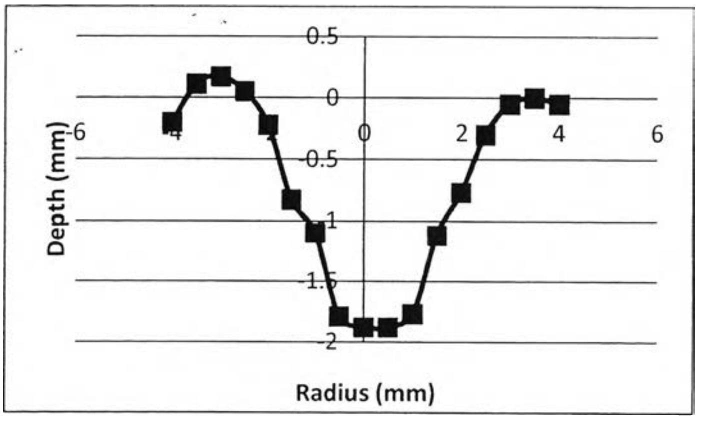


**Figure A.26** Potassium bitatrate profile at 160 ml/min and 20°C.

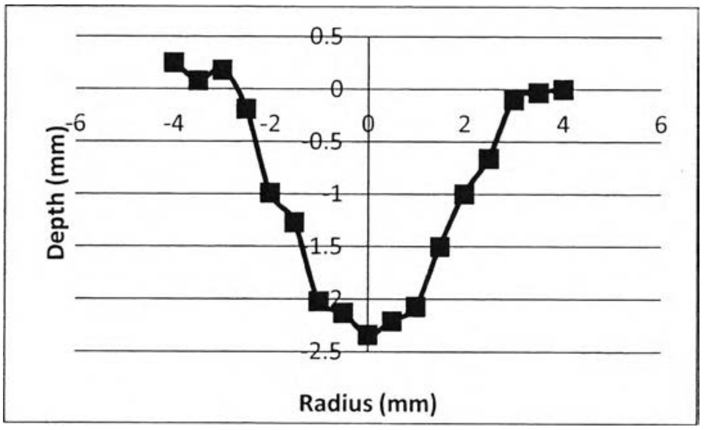


**Figure A.27** Potassium bitatrate profile at 180 ml/min and 20°C.

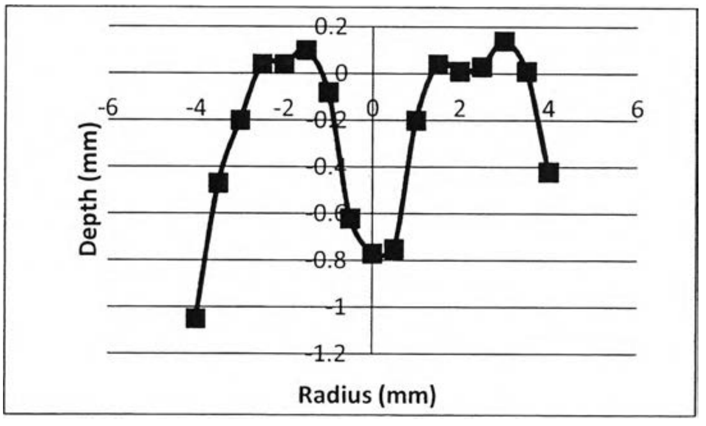


**Figure A.28** Aspartic acid profile at 40 ml/min and 20°C.

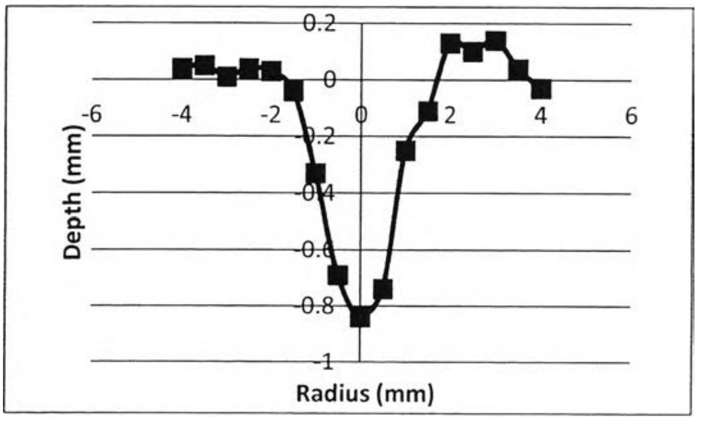


**Figure A.29** Aspartic acid profile at 60 ml/min and 20°C.

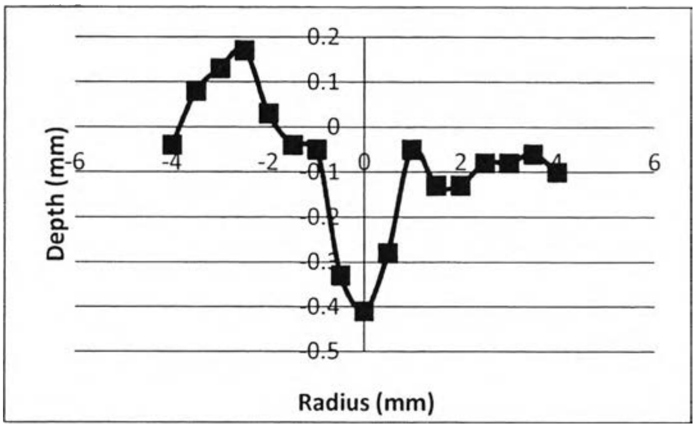


**Figure A.30** Aspartic acid profile at 80 ml/min and 20°C.

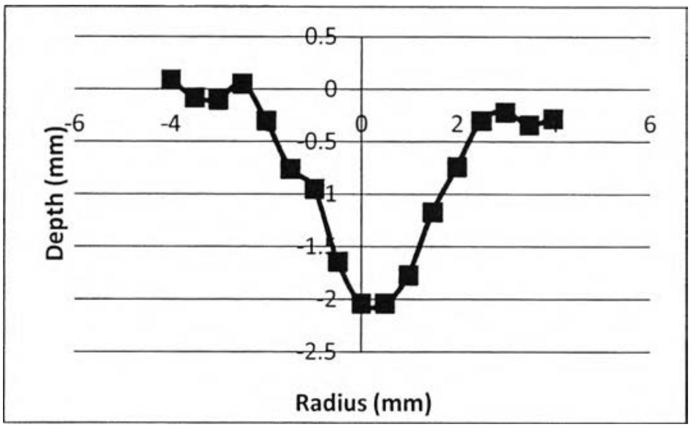


**Figure A.31** Aspartic acid profile at 100 ml/min and 20°C.

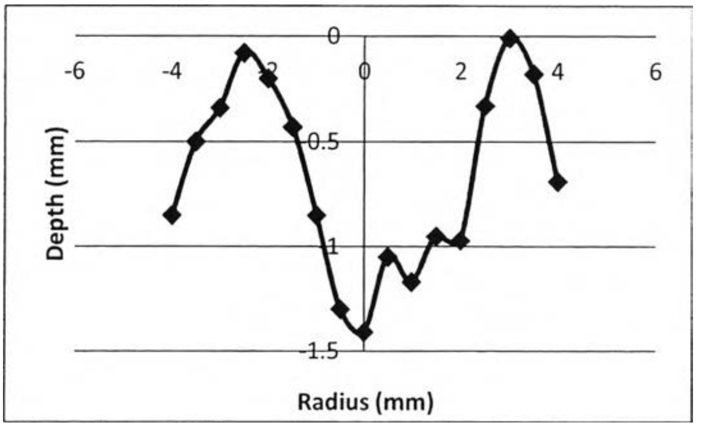


**Figure A.32** Aspartic acid profile at 120 ml/min and 20°C.

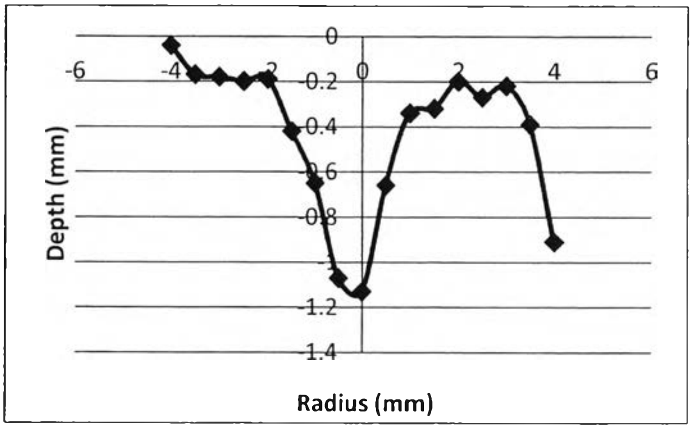


**Figure A.33** Aspartic acid profile at 140 ml/min and 20°C.

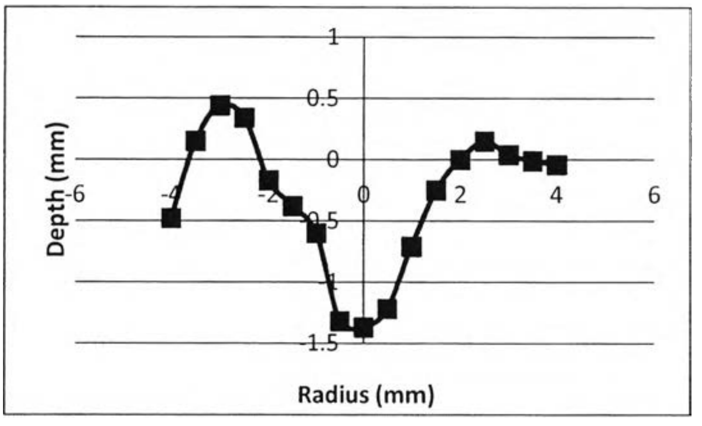


**Figure A.34** Aspartic acid profile at 160 ml/min and 20°C.

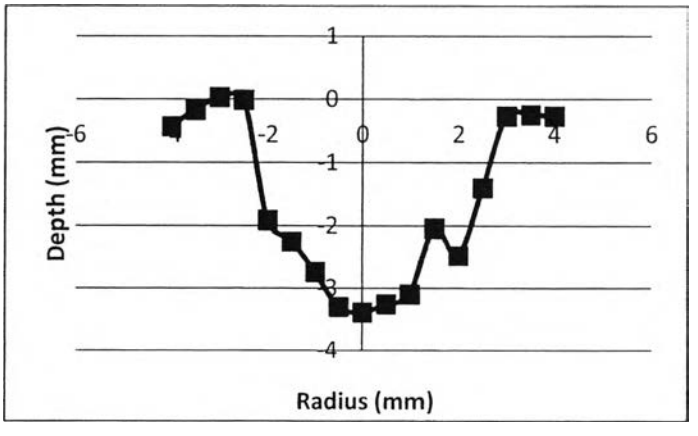


**Figure A.35** Aspartic acid profile at 180 ml/min and 20°C.

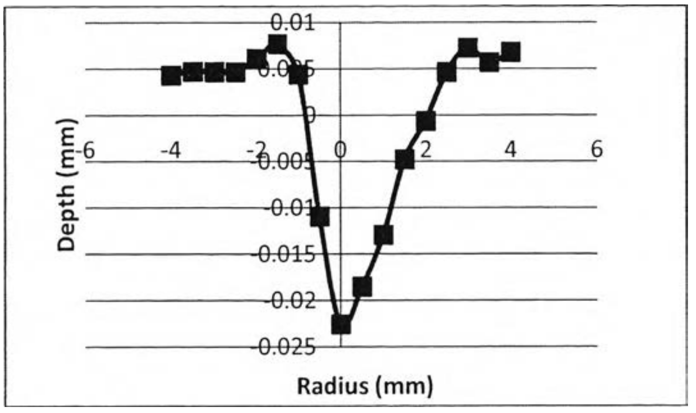


**Figure A.36** Trans-cinnamic acid profile at 40 ml/min and 20°C.

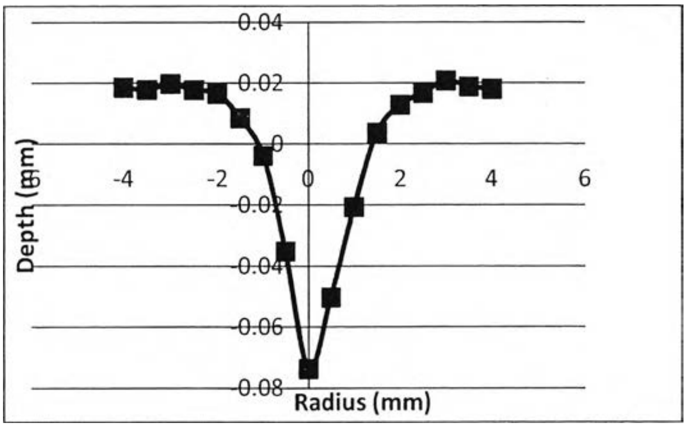


**Figure A.37** Trans-cinnamic acid profile at 60 ml/min and 20°C.

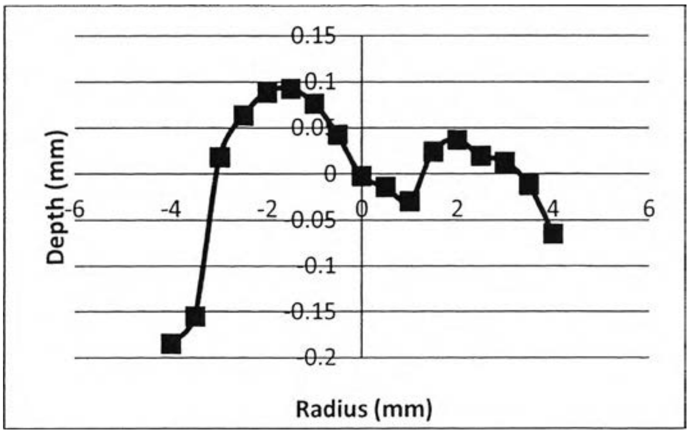


**Figure A.38** Trans-cinnamic acid profile at 80 ml/min and 20°C.

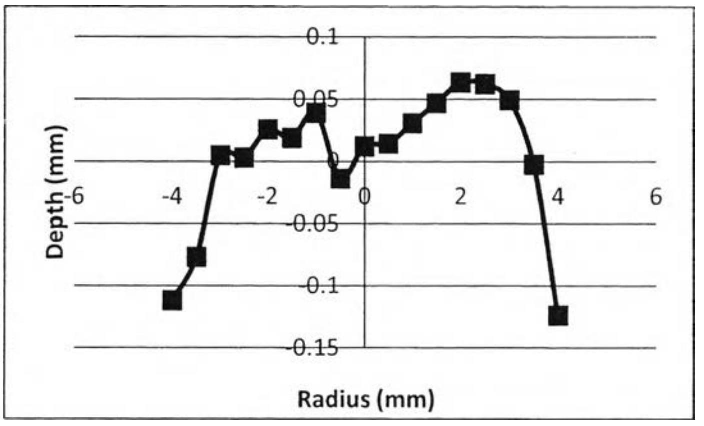


**Figure A.39** Trans-cinnamic acid profile at 100 ml/min and 20°C.

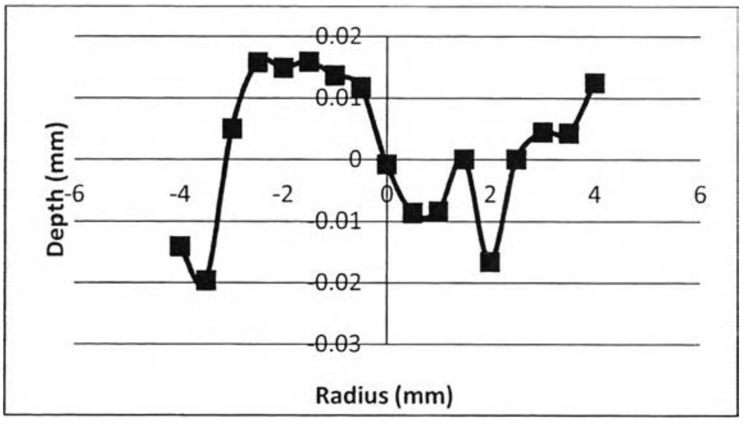


**Figure A.40** Trans-cinnamic acid profile at 120 ml/min and 20°C.

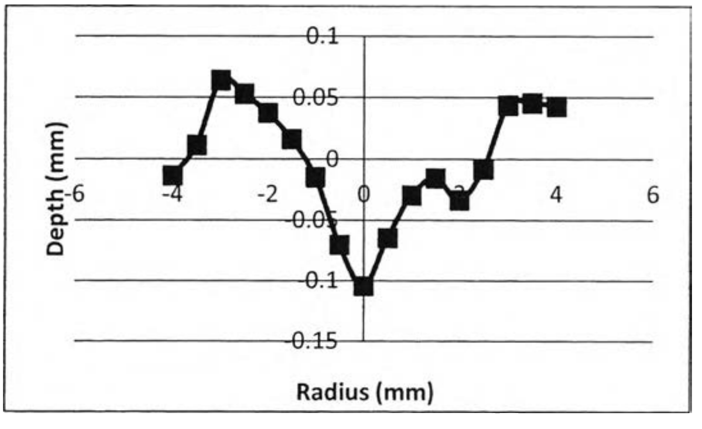


**Figure A.41** Trans-cinnamic acid profile at 140 ml/min and 20°C.

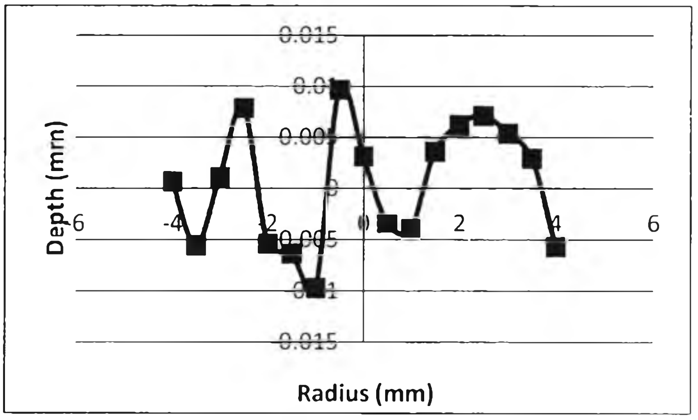


**Figure A.42** Trans-cinnamic acid profile at 160 ml/min and 20°C.

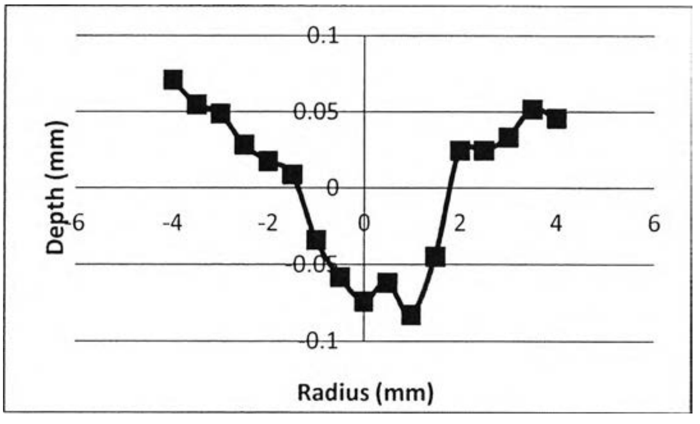


**Figure A.43** Trans-cinnamic acid profile at 180 ml/min and 20°C.

## Appendix B Thermophysical Properties of Water

Since our experiment carried out at different temperature, thermophysical properties of water were used to calculate Reynold number (Re) and Schmidt number (Sc), which led to determine the correlation of jet apparatus. The tabulated properties are pressure (P), density (ρ), enthalpy (H), entropy (S), isochoric heat capacity ($C_v$), isobaric heat capacity ($C_p$), speed of sound (u), viscosity (η), and thermal conductivity (Λ).

**Table B1** Thermophysical Properties of Water (CRC Handbook, 2011)

| T °C | P MPa | ρ kg/m$^3$ | H kJ/kg | S kJ/kgK | $C_v$ kJ/ kgK | $C_p$ kJ/kgK | u m/s | η μPas | Λ mW/ mK |
|---|---|---|---|---|---|---|---|---|---|
| 20 | 0 .1 | 998.2 | 84.0 | 0.3 | 4.2 | 4.2 | 1482.3 | 1001.6 | 598.6 |
| 25 | 0 .1 | 997.1 | 104.9 | 0.4 | 4.1 | 4.2 | 1496.7 | 890. 0 | 607.2 |
| 30 | 0 .1 | 995.7 | 125.8 | 0.4 | 4.1 | 4.2 | 1509.2 | 797.2 | 615.5 |
| 40 | 0 .1 | 992.2 | 167.6 | 0.6 | 4.1 | 4.2 | 1528.9 | 652.7 | 630.6 |

**Appendix C Diffusion at Infinite Dilution**

The diffusivities of materials were used to calculate Reynolds number (Re) in these experiments. The diffusion coefficient for a salt, $D_{salt}$, may be calculated from the $D^+$ and $D^-$ values of the constituent ions by the relation;

$$D_{salt} = \frac{(z_+ + |z_-|)D_+D_-}{z_+D_+ + |z_-|D_-}$$

where z is charge on the ion.

**Table C1** Diffusion at Infinite Dilution (CRC Handbook, 2011)

| Ion | D $10^{-5}cm^2s^{-1}$ | Ion | D $10^{-5}cm^2s^{-1}$ | Ion | D $10^{-5}cm^2s^{-1}$ |
|---|---|---|---|---|---|
| $Ag^+$ | 1.648 | $1/3La^{3+}$ | 0.619 | $Br^-$ | 2.080 |
| $1/3Al^{3+}$ | 0.541 | $Li^+$ | 1.029 | $Br_3^-$ | 1.145 |
| $1/2Ba^{2+}$ | 0.847 | $1/2Mg^{2+}$ | 0.706 | $BrO_3^-$ | 1.483 |
| $1/2Be^{2+}$ | 0.599 | $1/2Mn^{2+}$ | 0.712 | $CN^-$ | 2.077 |
| $1/2Ca^{2+}$ | 0.792 | $NH_4^+$ | 1.957 | $CNO^-$ | 1.720 |
| $1/2Cd^{2+}$ | 0.719 | $N_2H_5^+$ | 1.571 | $1/2CO_3^{2-}$ | 0.923 |
| $1/3Ce^{3+}$ | 0.620 | $Na^+$ | 1.334 | $Cl^-$ | 2.032 |
| $1/2Co^{2+}$ | 0.732 | $1/3Nd^{3+}$ | 0.616 | $ClO_2^-$ | 1.385 |
| $1/3[Co(NH3)_6]^{3+}$ | 0.904 | $1/2Ni^{2+}$ | 0.661 | $ClO_3^-$ | 1.720 |
| $1/3[Co(en)_3]^{3+}$ | 0.663 | $1/2Pb^{2+}$ | 0.945 | $ClO_4^-$ | 1.792 |
| $1/3Cr^{3+}$ | 0.595 | $1/3Pr^{3+}$ | 0.617 | $1/2CrO_4^{2-}$ | 1.132 |
| $Cs^+$ | 2.056 | $1/2Ra^{2+}$ | 0.889 | $F^-$ | 1.475 |
| $1/2Cu^{2+}$ | 0.714 | $Rb^+$ | 2.072 | $H_2AsO_4^-$ | 0.905 |
| $1/3Dy^{3+}$ | 0.582 | $1/3Sm^{3+}$ | 0.608 | $HF_2^-$ | 1.997 |
| $1/3Er^{3+}$ | 0.585 | $1/2Sr^{2+}$ | 0.791 | $1/2HPO_4^{2-}$ | 0.759 |
| $1/3Eu^{3+}$ | 0.602 | $Tl^+$ | 1.989 | $H_2PO_4^-$ | 0.959 |

**Table C1** (Con'td) Diffusion at Infinite Dilution (CRC Handbook, 2011)

| Ion | D $10^{-5}cm^2s^{-1}$ | Ion | D $10^{-5}cm^2s^{-1}$ |
|---|---|---|---|
| $I^-$ | 2.045 | $SeCN^-$ | 1.723 |
| $IO_3^-$ | 1.078 | $1/2SeO4^{2-}$ | 1.008 |
| $IO_4^-$ | 1.451 | $1/2WO4^{2-}$ | 0.919 |
| $MnO_4^-$ | 1.632 | Benzyltrimethylammonium$^+$ | 0.921 |
| $1/2MoO_4^{2-}$ | 1.984 | Isobutylammonium$^+$ | 1.012 |
| $N(CN)_2^-$ | 1.451 | Butyltrimethylammonium$^+$ | 0.895 |
| $NO_2^-$ | 1.912 | Decylpyridinium$^+$ | 0.786 |
| $NO_3^-$ | 1.902 | Decyltrimethylammonium$^+$ | 0.650 |
| $NH_2SO_3^-$ | 1.286 | Diethylammonium$^+$ | 1.118 |
| $N_3^-$ | 1.837 | Dimethylammonium$^+$ | 1.379 |
| $OCN^-$ | 1.720 | Dipropylammonium$^+$ | 0.802 |
| $OD^-$ | 3.169 | Dodecylammonium$^+$ | 0.634 |
| $OH^-$ | 5.273 | Dodecyltrimethylammonium$^+$ | 0.602 |
| $PF_6^-$ | 1.515 | Ethanolammonium$^+$ | 1.124 |
| $1/2PO_3F^{2-}$ | 0.843 | Ethylammonium$^+$ | 1.257 |
| $1/3PO_4^{3-}$ | 0.824 | Ethyltrimethylammonium$^+$ | 1.078 |
| $1/4P_2O_7^{4-}$ | 0.639 | Hexadecyltrimethylammonium$^+$ | 0.557 |
| $1/3P_3O_9^{3-}$ | 0.742 | Hexyltrimethylammonium$^+$ | 0.788 |
| $1/5P_3O_{10}^{5-}$ | 0.581 | Histidyl$^+$ | 0.612 |
| $ReO_4^-$ | 1.462 | Hydroxyethyltrimethylarsonium$^+$ | 1.049 |
| $SCN^-$ | 1.758 | Methylammonium$^+$ | 1.563 |
| $1/2SO_3^{2-}$ | 0.959 | Octadecylpyridinium$^+$ | 0.533 |
| $1/2SO_4^{2-}$ | 1.065 | Octadecyltributylammonium$^+$ | 0.442 |
| $1/2S2O_3^{2-}$ | 1.132 | Octadecyltriethylammonium$^+$ | 0.477 |
| $1/2S2O_4^{2-}$ | 0.885 | Octadecyltrimethylammonium$^+$ | 0.530 |

**Table C2** Diffusion at Infinite Dilution (CRC Handbook, 2011) Con'td.

| Ion | D $10^{-5}cm^2s^{-1}$ | Ion | D $10^{-5}cm^2s^{-1}$ |
|---|---|---|---|
| Octadecyltripropylammonium$^{+}$ | 0.458 | 1/2Malate$^{2-}$ | 0.783 |
| Octyltrimethylammonium$^{+}$ | 0.706 | 1/2Maleate$^{2-}$ | 0.824 |
| Pentylammonium$^{+}$ | 0.985 | 1/2Malonate$^{2-}$ | 0.845 |
| Piperidinium$^{+}$ | 0.991 | Methylsulfate$^{-}$ | 1.299 |
| Propylammonium$^{+}$ | 1.086 | Naphthylacetate$^{-}$ | 0.756 |
| Pyrilammonium$^{+}$ | 0.647 | 1/2Oxalate$^{2-}$ | 0.987 |
| Tetrabutylammonium$^{+}$ | 0.519 | Octylsulfate$^{-}$ | 0.772 |
| Tetradecyltrimethylammonium$^{+}$ | 0.573 | Phenylacetate$^{-}$ | 0.815 |
| Tetraethylammonium$^{+}$ | 0.868 | 1/2o–Phthalate$^{2-}$ | 0.696 |
| Tetramethylammonium$^{+}$ | 1.196 | 1/2m–Phthalate$^{2-}$ | 0.728 |
| Tetraisopentylammonium$^{+}$ | 0.477 | Picrate$^{-}$ | 0.809 |
| Tetrapentylammmonium$^{+}$ | 0.466 | Pivalate$^{-}$ | 0.849 |
| Tetrapropylammonium$^{+}$ | 0.623 | Propionate$^{-}$ | 0.953 |
| Triethylammonium$^{+}$ | 0.913 | Propylsulfate$^{-}$ | 0.988 |
| Triethylsulfonium$^{+}$ | 0.961 | Salicylate$^{-}$ | 0.959 |
| Trimethylammonium$^{+}$ | 1.258 | 1/2Suberate$^{2-}$ | 0.479 |
| Trimethylhexylammonium$^{+}$ | 0.921 | 1/2Succinate$^{2-}$ | 0.783 |
| Trimethylsulfonium$^{+}$ | 1.369 | p–Sulfonate | 0.780 |
| Tripropylammonium$^{+}$ | 0.695 | 1/2Tartarate$^{2-}$ | 0.794 |
| Acetate$^{-}$ | 1.089 | Trichloroacetate$^{-}$ | 0.932 |
| p–Anisate$^{-}$ | 0.772 | m–Chlorobenzoate$^{-}$ | 0.825 |
| 1/2Azelate$^{2-}$ | 0.541 | o–Chlorobenzoate$^{-}$ | 0.804 |
| Benzoate$^{-}$ | 0.863 | 1/3Citrate$^{3-}$ | 0.623 |
| Bromoacetate$^{-}$ | 1.044 | Crotonate$^{-}$ | 0.884 |
| Bromobenzoate$^{-}$ | 0.799 | Cyanoacetate$^{-}$ | 1.156 |

**Appendix D Transformations of the coordinates**

The dissolution areas of this study were calculated Surface Integrals area; follow by this equation;

$$\iint_s f(x,y,z)ds = \iint_d f((x,y,z(x,y))\sqrt{\left(\frac{\partial z}{\partial x}\right)^2 + \left(\frac{\partial z.n}{\partial y}\right)^2 + 1}dA \quad \text{(D-1)}$$

Thus a cylindrical coordinate system and Cartesian coordinate system are observed (Welty et al., 2007);

$$\left(\frac{\partial}{\partial z}\right)_{cyl} = \left(\frac{\partial}{\partial z}\right)_{cart} \quad \text{(D-2)}$$

whereas, from the chain rule

$$\left(\frac{\partial}{x}\right) = \frac{\partial}{\partial r}\frac{\partial r}{\partial x} + \frac{\partial}{\partial \theta}\frac{\partial \theta}{\partial x} \quad \text{(D-3)}$$

thus

$$\left(\frac{\partial}{\partial x}\right) = cos\theta\left(\frac{\partial}{\partial r}\right) - \frac{\sin\theta}{r}\left(\frac{\partial}{\partial \theta}\right) \quad \text{(D-4)}$$

In similar manner,

$$\left(\frac{\partial}{y}\right) = \frac{\partial}{\partial r}\frac{\partial r}{\partial y} + \frac{\partial}{\partial \theta}\frac{\partial \theta}{\partial y} \quad \text{(D-5)}$$

where

$$\left(\frac{\partial r}{\partial y}\right) = \frac{y}{r} = sin\theta \text{ and } \frac{\partial \theta}{\partial y} = \frac{1}{xsec^2\theta} = \frac{cos\theta}{r}$$

Thus, $(\partial/\partial y)$ becomes

$$\left(\frac{\partial}{\partial y}\right) = sin\theta\left(\frac{\partial}{\partial r}\right) + \frac{\cos\theta}{r}\left(\frac{\partial}{\partial \theta}\right) \quad \text{(D-5)}$$

So Equation D-1 becomes

$$\text{Area}=\int_0^\theta \int_0^r \left[\sqrt{\left(cos\theta\frac{dz}{dr} - \frac{1}{r}\sin\theta\frac{dz}{d\theta}\right)^2 + \left(\sin\theta\frac{dz}{dr} + \frac{1}{r}\cos\theta\,\theta\frac{dz}{d\theta}\right)^2 + 1}\right] rdrd\theta \quad \text{(D-6)}$$

where z is the depth at r position and θ is angle at r position.

# CURRICULUM VITAE

**Name:** Ms. Thanutchaphorn Phupongskorn

**Date of Birth:** July 11, 1988

**Nationality:** Thai

**University Education:**

2006–2010 Bachelor Degree of Chemical Engineering, Faculty of Engineering, King Mongkut's University of Technology North Bangkok, Bangkok, Thailand

**Work Experience:**

| | | |
|---|---|---|
| 2009 | Position: | Engineer Internship Student |
| | Company: | Fuji Shinsei Co., Ltd, Pathumtani, Thailand |
| 2011-2012 | Position: | Research Assitant |
| | Company name: | Nuclear Group, University of New Brunswick, Fredericton, New Brunswick, Canada |

**Presentations:**

1. Thanutchaphorn P., Lister, D.H., Steward, F.R., and Rirksomboon, T. (2012, April 24) Determination of Dissolution of a Material with a Moderately-rapid Dissolution Rate. Poster presented at The $3^{th}$ Research Symposium on Petroleum, Petrochemicals, and Advanced Materials and the $18^{th}$ PPC Symposium on Petroleum, Petrochemicals, and Polymers, Bangkok, Thailand.